NUCLEAR THEORY, Vol. 36 (2017)
eds. M. Gaidarov, N. Minkov, Heron Press, Sofia

Proton-Halo Nature of the ^{8}B Nucleus Through Studies of Elastic Scattering and Breakup Reactions

M.K. Gaidarov[1], **V.K. Lukyanov**[2], **D.N. Kadrev**[1],
E.V. Zemlyanaya[2], **K.V. Lukyanov**[2], **A.N. Antonov**[1], **K. Spasova**[1]

[1]Institute for Nuclear Research and Nuclear Energy,
Bulgarian Academy of Sciences, Sofia 1784, Bulgaria
[2]Joint Institute for Nuclear Research, Dubna 141980, Russia

Abstract. A microscopic analysis of the optical potentials (OPs) and cross sections of elastic scattering of ^{8}B on ^{12}C, ^{58}Ni, and ^{208}Pb targets at energies $20 < E < 170$ MeV is carried out. The real part of the OP is calculated by a folding procedure and the imaginary part is obtained on the base of the the high-energy approximation (HEA). The density distributions of ^{8}B obtained within the variational Monte Carlo (VMC) model and the three-cluster model (3CM) are used to construct the potentials. In this hybrid model, the only free parameters are the depths of the real and imaginary parts of OP obtained by fitting the experimental data. The use of HEA to estimate the imaginary OP at energies just above the Coulomb barrier is discussed. The analysis of the behavior of 3CM and VMC densities and the corresponding OPs in comparison with the fitted Woods-Saxon OP gives additional information on the decisive role of the nuclear surface on the elastic scattering mechanism in the particular example of ^{8}B+^{58}Ni cross sections measured in a wide range of angles and at energies of 20.7, 23.4, 25.3, 27.2, and 29.3 MeV. In addition, a cluster model, in which ^{8}B consists of a p-halo and the ^{7}Be core, is applied to calculate the breakup cross sections of ^{8}B nucleus on ^{9}Be, ^{12}C, and ^{197}Au targets, as well as the momentum distributions of ^{7}Be fragments. A good agreement of the theoretical results with the available experimental data is obtained.

1 Introduction

The scattering of nuclei away from the nuclear stability line has been one of the principal fields of research in low-energy nuclear physics in recent decades. In particular, the light exotic nuclei present unusual features. Neutron halos, consisting of extended neutron distributions coupled to a core, have been found for many weakly bound neutron-rich nuclei such as ^{11}Li and ^{11}Be [1, 2]. These weakly bound nuclei have a strongly clusterized structure [3–6]. In a simple model, they are seen as a core, that contains most of the nucleons, to which one or two neutrons are loosely bound. The latter is related to the tunneling of the valence neutrons far outside the classically allowed region which form a sort of halo around the core [7, 8].

The proton drip-line nucleus ^{8}B, with a proton separation energy of 0.137 MeV, has attracted intense experimental and theoretical attention because it is the most likely a nucleus with a proton halo. Moreover, this nucleus is valuable for astrophysical reasons [9, 10]. The narrow momentum distributions of ^{7}Be fragments in the breakup of ^{8}B measured in C, Al, and Pb targets at 1471 MeV/nucleon with full width at half maximum (FWHM) of 81 ± 6 MeV/c in all targets have been interpreted in terms of a largely extended proton distribution for ^{8}B and have implied a radius of 2.78 fm [11]. As the narrow longitudinal momentum distribution of the ^{7}Be fragment from breakup reactions is regarded as prominent evidence of an extended structure of ^{8}B, many measurements of the ^{7}Be longitudinal momentum distributions have been performed. Here we should mention the results of the experiments at lower energies for the breakup of ^{8}B in the collisions with Be and Au targets at 41 MeV/nucleon (81 ± 4 and 62 ± 3 MeV/c FWHM for Be and Au targets, respectively) [12] and for C target at 36 MeV/nucleon [13] with FWHM 124 ± 17 and 92 ± 7 MeV/c for the stripping and diffraction components, correspondingly. Indeed, these experimental results reflect the large spatial extension of the loosely bound proton in ^{8}B. The halo nature of ^{8}B nucleus through studies of its breakup has been mostly tested with cluster models presuming simple two-cluster structure that consists of ^{7}Be core and valence proton (for instance, Refs. [11, 14]).

The aims of the present work (see also [15]) are as follows. First, we analyze the differential elastic cross sections for the scattering of ^{8}B on ^{12}C at 25.8 MeV [16], ^{8}B on ^{58}Ni at 20.7, 23.4, 25.3, 27.2, and 29.3 MeV [17], and ^{8}B on ^{208}Pb at 170.3 MeV [18] within the microscopic model of the respective OP and compare the results with the available experimental data. As in our previous works [19–23], where processes with neutron-rich He, Li, and Be isotopes were considered, we use the hybrid model of OP [24], in which the real part (ReOP) is calculated by a folding of a nuclear density and the effective nucleon-nucleon (NN) potentials [25] and includes direct and exchange isoscalar and isovector parts. The imaginary part (ImOP) is obtained on the base of the high-energy approximation method developed in Refs. [26, 27]. There are only two fitting parameters in the hybrid model, which are related to the depths of the ReOP and ImOP. In the present work we use the density distribution of ^{8}B nucleus obtained within the variational Monte Carlo model [28] and also the density obtained within the framework of the microscopic three-cluster model of Varga *et al.* [29]. Second, we calculate the momentum distributions of ^{7}Be fragments from the breakup reactions ^{8}B+^{9}Be, ^{8}B+^{12}C, and ^{8}B+^{197}Au for which experimental data are available. Such a complex study based on the microscopic method to obtain the OPs with a minimal number of free parameters and by testing density distributions of ^{8}B which reflect its proton-halo structure (in contrast, e.g., to the Hartree-Fock density used in Ref. [18]) would lead to a better understanding of the ^{8}B structure.

2 Elastic Scattering of ^{8}B on ^{12}C, ^{58}Ni, and ^{208}Pb

The microscopic volume OP used in our calculations contains the real part (V^{DF}) including both the direct and exchange terms and the HEA microscopically calculated imaginary part (W^H). It has the form

$$U(r) = N_R V^{DF}(r) + iN_I W^H(r). \tag{1}$$

The parameters N_R and N_I entering Eq. (1) renormalize the strength of OP and are fitted by comparison with the experimental cross sections. The real part V^{DF} consists of the direct (V^D) and exchange (V^{EX}) double-folding integrals that include effective NN potentials and density distribution functions of colliding nuclei. The V^D and V^{EX} parts of the ReOP have isoscalar (IS) and isovector (IV) contributions. The IS ones of both terms are:

$$V_{IS}^D(r) = \int d^3r_p d^3r_t \rho_p(\mathbf{r}_p)\rho_t(\mathbf{r}_t) v_{NN}^D(s), \tag{2}$$

$$V_{IS}^{EX}(r) = \int d^3r_p d^3r_t \rho_p(\mathbf{r}_p, \mathbf{r}_p + \mathbf{s})\rho_t(\mathbf{r}_t, \mathbf{r}_t - \mathbf{s}) \times v_{NN}^{EX}(s) \exp\left[\frac{i\mathbf{K}(r)\cdot s}{M}\right], \tag{3}$$

where $\mathbf{s} = \mathbf{r} + \mathbf{r}_t - \mathbf{r}_p$ is the vector between two nucleons, one of which belongs to the projectile and another one to the target nucleus. In Eq. (2) $\rho_p(\mathbf{r}_p)$ and $\rho_t(\mathbf{r}_t)$ are the densities of the projectile and the target, respectively, while in Eq. (3) $\rho_p(\mathbf{r}_p, \mathbf{r}_p+\mathbf{s})$ and $\rho_t(\mathbf{r}_t, \mathbf{r}_t-\mathbf{s})$ are the density matrices for the projectile and the target that are usually taken in an approximate form. The effective NN interactions v_{NN}^D and v_{NN}^{EX} have their IS and IV components in the form of M3Y interaction obtained within g-matrix calculations using the Paris NN potential [25]. The expressions for the energy and density dependence of the effective NN interaction are given, e.g., in Ref. [23].

Concerning the ImOP, it corresponds to the full microscopic OP derived in Refs. [24, 30] within the HEA [26, 27]:

$$W^H(r) = -\frac{1}{2\pi^2}\frac{E}{k}\bar{\sigma}_N \int_0^\infty j_0(qr)\rho_p(q)\rho_t(q) f_N(q) q^2 dq. \tag{4}$$

In Eq. (4) $\rho(q)$ are the corresponding form factors of the nuclear densities, $f_N(q)$ is the amplitude of the NN scattering and $\bar{\sigma}_N$ is the averaged over the isospin of the nucleus total NN scattering cross section that depends on the energy and accounts for the in-medium effect.

To apply the microscopic OPs to scattering of ^{8}B on nuclei we used realistic density distributions of ^{8}B calculated within the VMC model [28] and from the 3CM in Ref. [29]. In our case, within the VMC method the proton and neutron densities have been computed with the AV18+UX Hamiltonian, in which the Argonne v18 two-nucleon and Urbana X three-nucleon potentials are used [28].

Urbana X is intermediate between the Urbana IX and Illinois-7 models (the latter was used by us in Ref. [23] for the densities of ^{10}Be nucleus). As far as the 3CM densities of Varga *et al.* [29] are concerned, the ^{8}B nucleus has been studied in a microscopic α+h+p three-cluster model (h=^{3}He) using the stochastic variational method, where a Minnesota effective two-nucleon interaction was used. It has been shown in [29] that the proton separation energy of ^{8}B is reasonably reproduced, but the calculated point matter radius exceeds the "empirical" one. The VMC and 3CM densities are given in Figure 1. It can be seen that they have been calculated with enough accuracy up to distances much larger than the nuclear radius. In both methods the total densities of ^{8}B occur quite similar up to $r \sim 4$ fm and a difference between them is seen in their periphery. Due to the cluster-structure model of ^{8}B, where the proton is considered as a single cluster [29], the tail part of the point-proton distribution of ^{8}B is significantly larger than that of the neutron one, causing considerable difference in the corresponding rms radii (see Ref. [15]).

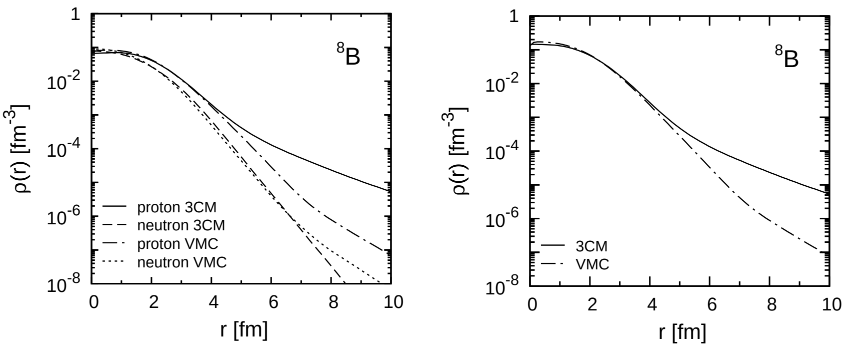

Figure 1. Point-proton (normalized to Z=5), point-neutron (normalized to N=3) (left panel) and the total densities (right panel) of ^{8}B (normalized to A=8) obtained in the VMC method [28] and in the 3CM [29].

The calculated within the hybrid model elastic scattering cross sections of ^{8}B+^{12}C at energy $E = 25.8$ MeV in the laboratory frame are given in Figure 2 and compared with the experimental data [16]. It can be seen that in both cases of calculations with VMC or 3CM densities the results are in good agreement with the available data. The differential cross section obtained with VMC density demonstrates more developed diffractional picture. It would be desirable to measure the elastic scattering in the angular range beyond 55°, where the differences between the theoretical results start, in order to determine the advantage of using VMC or 3CM microscopic densities of ^{8}B. Complementary measurements at smaller steps of scattering angle would also allow one to observe some possible oscillations of the cross section. Our next step was to study ^{8}B elastic scattering on a lead target at 170.3 MeV incident energy. The same Figure 2 shows a fair agreement of our microscopic calculations with the experimental

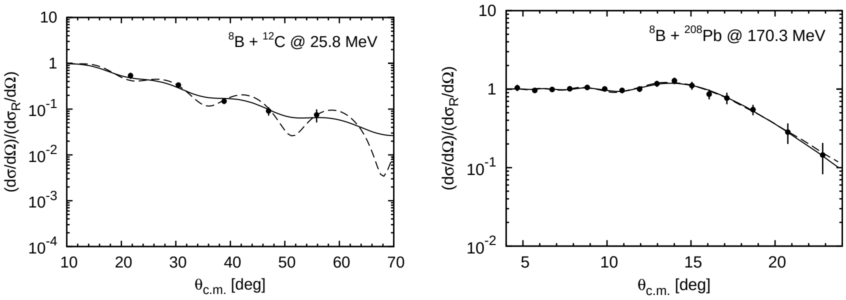

Figure 2. (Left) ^{8}B+^{12}C elastic scattering cross sections at $E = 25.8$ MeV. Solid line: calculations with 3CM density of ^{8}B; dashed line: calculations with VMC density of ^{8}B. Experimental data are taken from Ref. [16]; (Right) ^{8}B+^{208}Pb elastic scattering cross sections at $E = 170.3$ MeV. Solid line: calculations with 3CM density of ^{8}B; dashed line: calculations with VMC density of ^{8}B. Experimental data are taken from Ref. [18].

data for the cross section. Both VMC and 3CM densities used in the calculations are able to reproduce the data that are restricted in a range of small angles. Similarly to the case of ^{8}B+^{12}C process, the reasonable agreement of our model with the data on ^{8}B+^{208}Pb elastic scattering is in favor of the very weak contribution from other reaction mechanisms, which is supported by the results from CDCC calculations [16, 18].

In what follows, we present in Figure 3 (left panel) our results for ^{8}B+^{58}Ni elastic scattering cross sections at energies 20.7, 23.4, 25.3, 27.2, and 29.3 MeV using the VMC density. These results are obtained with N_R and N_I which reproduce in a best way the experimental cross sections at considered five energies. One can see that the results are in a good agreement with the data for all energies considered. It is well known that the couplings to non-elastic channels lead to polarization potentials that can considerably modify the bare potential calculated within the double folding formalism. Obviously, for more successful description of cross sections at low energies near Coulomb barrier an inclusion of polarization contributions due to virtual excitations and decay channels of the reactions is necessary to obtain unambiguously the OP renormalization parameters. The good fit obtained for the experimental angular distributions in Ref. [17] with real and imaginary potentials of the Woods-Saxon type and our best fit to the same data using microscopic OP in this work lead to values of the predicted total reaction cross section σ_R very close to each other (see [15]), the latter exhibiting a smooth increase with the energy increase.

Also, we give in Figure 3 (right panel), as an example (for $E = 29.3$ MeV), the comparison of the obtained real and imaginary parts of the OPs for both 3CM and VMC densities with the corresponding parts of the fitted Woods-Saxon potential used in [17]. The values of our parameters N_R and N_I are indicated in the figure. Here we mention that at such energies the surface part of the ImOP plays a decisive role on the behavior of the elastic cross sections. One can see

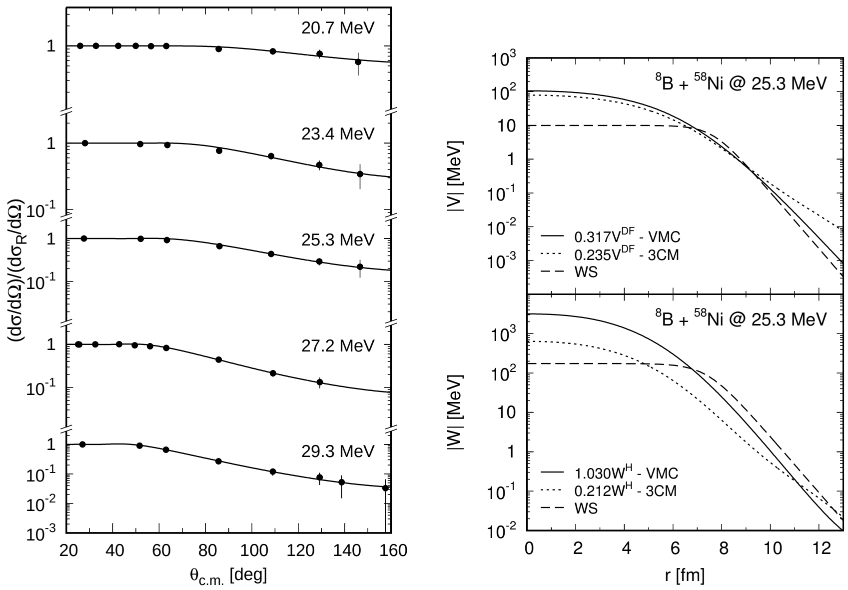

Figure 3. (Left) ^{8}B+^{58}Ni elastic scattering cross sections at $E = 20.7, 23.4, 25.3, 27.2$ and 29.3 MeV calculated using the VMC density of ^{8}B. Experimental data are taken from Ref. [17]; (Right) The absolute values of the real $N_R V^{DF}$ and imaginary $N_I W^H$ parts of the calculated optical potentials for the ^{8}B+^{58}Ni elastic scattering at $E = 29.3$ MeV obtained using the VMC and 3CM densities of ^{8}B in comparison with those of the WS potential from Ref. [17].

that the use of the VMC density leads to a very good agreement of the imaginary part of our OP with the imaginary part of the fitted WS OP in the surface region. Also, the slope of the real part of OP obtained with the VMC density in this region ($8 < r < 10$ fm) is similar to that of the real part of WS OP. There exist some differences in the surface region for the real and imaginary parts of the OP obtained with the 3CM density and the corresponding parts of the WS OP.

3 Breakup Processes of ^{8}B

In this section we consider the characteristics of breakup processes of the ^{8}B nucleus on the example of the stripping reaction cross sections and the momentum distributions of the fragments. We use a model in which ^{8}B consists of a core of ^{7}Be and a halo of a single proton (see, e.g., Refs. [11]). In this model the density of ^{7}Be has to be known. We use that one obtained from the calculations performed by means of the 3CM density of ^{8}B [29].

For calculations of breakup cross sections and momentum distributions of fragments in the ^{7}Be+p breakup model within the eikonal formalism (see, e.g. Ref. [31]), one needs the expressions of the S-matrix (as a function of the impact parameter b):

$$S(b) = \exp\left[-\frac{i}{\hbar v}\int_{-\infty}^{\infty} U^{(b)}(\sqrt{b^2+z^2})dz\right], \tag{5}$$

where

$$U^{(b)} = V + iW \tag{6}$$

is the OP of the breakup of ^{8}B in its collision with nuclear targets within the ^{7}Be+p cluster model. The longitudinal momentum distribution of ^{7}Be fragments produced in the breakup of ^{8}B in the case of stripping reaction (when the proton leaves the elastic channel) is (more details can be found in Ref. [15])

$$\left(\frac{d\sigma}{dk_L}\right)_{str} = \frac{1}{3}\int_0^{\infty} b_p db_p \left[1 - |S_p(b_p)|^2\right] \times \int \rho d\rho d\varphi_\rho |S_c(b_c)|^2 \sum_{m=0,\pm 1} F_m(\rho). \tag{7}$$

The wave function of the relative motion of the proton and ^{7}Be clusters in ^{8}B is obtained by solving the Schrödinger equation with the Woods-Saxon potential for a particle with a reduced mass of two clusters. The parameters of the WS potentials are obtained by a fitting procedure, namely, to reach the proton separation energy $S_p = 137$ KeV. However, this procedure could provide several sets of potential parameters that satisfy the above condition. They are close to each other leading, at the same time, to different valence proton rms radii. Therefore, in order to understand better the observed widths of the longitudinal momentum distributions of ^{7}Be fragments formed in the breakup of ^{8}B and measured at different targets and energies, we consider three cases. The values of WS potential parameters and corresponding rms radii of the cluster formation for $1p$ state in which the valence proton in ^{8}B is mainly bound (see Refs. [14, 31]) are listed in Table 1.

The stripping cross sections for reactions ^{8}B+^{9}Be, ^{8}B+^{12}C, and ^{8}B+^{197}Au are calculated from Eq. (7). The obtained results are illustrated in Figure 4. The blue dotted, black solid, and red dashed curves in the figures correspond to the three sets of WS parameters given in Table 1.

Table 1. The parameters V_0 (in MeV), R (in fm), a (in fm) of the Woods-Saxon potentials and the rms radii of the cluster wave function (in fm) obtained by using of the 3CM density of ^{7}Be for three cases (see the text).

V_0	R	a	rms radii
38.22	2.70	0.55	4.51
38.70	2.50	0.20	5.08
38.77	2.48	0.50	6.24

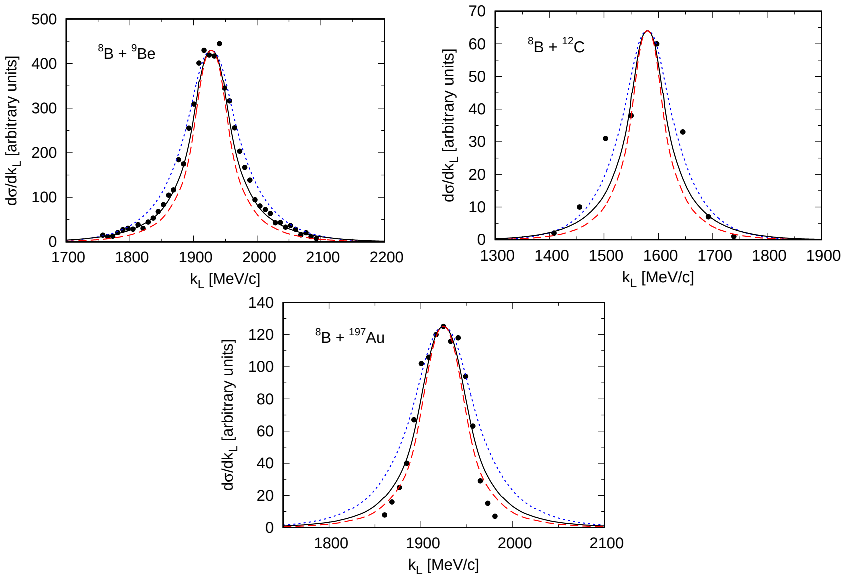

Figure 4. Cross sections of stripping reactions in ^{8}B+^{9}Be scattering at $E = 41$ MeV/nucleon, ^{8}B+^{12}C scattering at $E = 36$ MeV/nucleon, and ^{8}B+^{197}Au scattering at $E = 41$ MeV/nucleon. Experimental data are taken from Refs. [12], [13], and [12], respectively.

It is worth to note the relevance between the rms radii of the wave function of the ^{7}Be-p relative motion and the obtained FWHMs for the considered three cases. Due to the uncertainty principle the widths become smaller with the increase of the distance between two clusters. We note the good agreement with the experimental data from light and heavy breakup targets. It can be seen from Figure 4 that the best agreement with the experimental data for the parallel momentum distributions of ^{7}Be fragments in a breakup reaction of ^{8}B on a ^{9}Be target at 41 MeV/nucleon and on a ^{12}C target at 36 MeV/nucleon is achieved when the relative ^{7}Be-proton distance is 5.08 fm or 4.51 fm, respectively, while in the case of ^{8}B breakup on a ^{197}Au target at 41 MeV/nucleon shown in the same figure a larger distance (6.24 fm) is needed to get better coincidence with the data. The values of the theoretical FWHMs in this case are 72.07 MeV/c when describing the stripping mechanism of the ^{8}B breakup on the ^{9}Be target, 108.71 MeV/c for the breakup on ^{12}C target, and 54.86 in the case of ^{197}Au target. These values are close to the experimentally measured widths and are within the range found in other theoretical analyses.

We note that from the comparison of the results in the present work with those obtained in our previous works [22, 23] for the cases of ^{11}Li and ^{11}Be breakup, it can be concluded that the halo cluster ($2n$ or n) in these nuclei can be found outside the core with larger probability than the valence proton in ^{8}B.

This observation together with the variation of the width with target in breakup reactions of ^{8}B at almost equal energies show the specific features of the momentum distributions of corelike fragments in breakup of neutron and proton halo nuclei.

4 Summary and Conclusions

In the present work (see also [15]) we performed microscopic calculations of the optical potentials and cross sections of elastic scattering ^{8}B+^{12}C at 25.8 MeV, ^{8}B+^{58}Ni at 20.7, 23.4, 25.3, 27.2, and 29.3 MeV, and ^{8}B+^{208}Pb at 170.3 MeV, in comparison with the available experimental data. The direct and exchange isoscalar and isovector parts of the real OP (V^{DF}) were calculated microscopically using the double-folding procedure and density dependent M3Y (CDM3Y6-type) effective interaction based on the Paris NN potential. The imaginary part of the OP (W^H) was calculated within the HEA. Two model microscopic densities of protons and neutrons in ^{8}B were used in the calculations: the density calculated within the VMC model [28] and from the three-cluster model [29]. In this way, in contrast to the phenomenological and semi-microscopic models we deal with a fully microscopic approach as a physical ground to account for the single-particle structure of the colliding nuclei.

We have tested our microscopic model studying the role of the breakup mechanism to analyze properly the whole picture of ^{8}B scattering. For this purpose, we use another folding approach to consider the ^{8}B breakup by means of the simple ^{7}Be+p cluster model for the structure of ^{8}B. We calculate in HEA the ImOP of the interaction of ^{7}Be with the target, as well as the p+target interaction. Using them the corresponding S-matrices for the core and proton within the eikonal formalism are obtained. The latter are used to get results for the longitudinal momentum distributions of ^{7}Be fragments produced in the breakup of ^{8}B on different targets. This includes the breakup reactions of ^{8}B on ^{9}Be and ^{197}Au at $E = 41$ MeV/nucleon and ^{8}B on ^{12}C at $E = 36$ MeV/nucleon, for which a good agreement of our calculations for the stripping reaction cross sections with the available experimental data were obtained. The theoretical widths are close to the empirical ones.

In general, we can conclude that our microscopic approach can be applied to reaction studies with exotic nuclei such as ^{8}B. The consistency of our results with the measured elastic cross sections and narrow longitudinal momentum distributions may provide supplemental information on the internal spatial structure of the ^{8}B nucleus supporting its proton-halo nature.

Acknowledgements

Four of the authors (D.N.K., A.N.A., M.K.G. and K.S.) are grateful for the support of the Bulgarian Science Fund under Contracts Nos. DFNIT02/19 and DNTS/Russia 01/3 and one of them (D.N.K.) under Contract No. DFNIE02/6.

The authors V.K.L., E.V.Z. and K.V.L. thank to the Russian Foundation for Basic Research (Grant N17-52-18057-bolg-a) for the partial support.

References

[1] I. Tanihata *et al.*, *Phys. Lett. B* **160** (1985) 380-384.
[2] I. Tanihata *et al.*, *Phys. Rev. Lett.* **55** (1985) 2676-2679.
[3] P.G. Hansen, A.S. Jensen, and B. Jonson, *Annu. Rev. Nucl. Part. Sci.* **45** (1995) 591-634.
[4] I. Tanihata, *J. Phys. G* **22** (1996) 157-198.
[5] B. Jonson, *Phys. Rep.* **389** (2004) 1-59.
[6] G. Baur, K. Hencken, and D. Trautmann, *Prog. Part. Nucl. Phys.* **51** (2003) 487-564.
[7] A.B. Migdal, *Yad. Fiz.* **16** (1972) 427-434; *Sov. J. Nucl. Phys.* **16**(1973) 238-241.
[8] P.G. Hansen and B. Jonson, *Europhys. Lett.* **4** (1987) 409-414.
[9] B. Davids *et al.*, *Phys. Rev. Lett.* **81** (1998) 2209-2212.
[10] L. Trache *et al.*, *Phys. Rev. C* **67** (2003) 062801.
[11] W. Schwab *et al.*, *Z. Phys. A* **350** (1995) 283-284.
[12] J.H. Kelley *et al.*, *Phys. Rev. Lett.* **77** (1996) 5020-5023.
[13] S.L. Jin *et al.*, *Phys. Rev. C* **91** (2015) 054617.
[14] H. Esbensen, *Phys. Rev. C* **53** (1996) 2007-2010.
[15] V.K. Lukyanov, D.N. Kadrev, E.V. Zemlyanaya, K.V. Lukyanov, A.N. Antonov, M.K. Gaidarov, and K. Spasova, *Eur. Phys. J. A* **53** (2017) 31.
[16] A. Barioni *et al.*, *Phys. Rev. C* **84** (2011) 014603.
[17] E.F. Aguilera *et al.*, *Phys. Rev. C* **79** (2009) 021601(R).
[18] Y.Y. Yang *et al.*, *Phys. Rev. C* **87** (2013) 044613.
[19] K.V. Lukyanov *et al.*, *Eur. Phys. J. A* **33** (2007) 389-400.
[20] V.K. Lukyanov *et al.*, *Phys. Rev. C* **80** (2009) 024609.
[21] V.K. Lukyanov *et al.*, *Phys. Rev. C* **82** (2010) 024604.
[22] V.K. Lukyanov *et al.*, *Phys. Rev. C* **88** (2013) 034612.
[23] V.K. Lukyanov *et al.*, *Phys. Rev. C* **91** (2015) 034606.
[24] K.V. Lukyanov, E.V. Zemlyanaya, and V.K. Lukyanov, *Phys. At. Nucl.* **69** (2006) 240-254.
[25] D.T. Khoa and G.R. Satchler, *Nucl. Phys. A* **668** (2000) 3-41.
[26] R.J. Glauber, In: *Lectures in Theoretical Physics* (Interscience, New York, 1959) p. 315.
[27] A.G. Sitenko, *Ukr. Fiz. J.* **4** (1959) 152-163.
[28] S.C. Pieper, private communication.
[29] K. Varga, Y. Suzuki, and I. Tanihata, *Phys. Rev. C* **52** (1995) 3013-3026.
[30] P. Shukla, *Phys. Rev. C* **67** (2003) 054607.
[31] K. Hencken, G. Bertsch, and H. Esbensen, *Phys. Rev. C* **54** (1996) 3043-3050.